

# High-precision 3D measurements on moving objects

Matthias Laimer\*, Daniel Wertjanz\*, Peter Gsellmann, Georg Schitter, *Senior Membership, IEEE* and Ernst Csencsics

**Abstract**—This paper presents a 6-DOF dual stage sample-tracking system for compensating relative motion and enabling high precision 3D surface measurements on moving objects. The system comprises a 3D measurement module for fine positioning, which is mounted as end effector to an industrial robot being used for coarse positioning. The embedded free-floating measurement platform actively tracks a sample to locally establish lab-like conditions for the integrated 3D measurement tool. A dual stage position control scheme is designed to dynamically reposition the long-range actuator for tracking a moving sample, such that the measurement platform is kept within its actuation range. Experiments on a moving sample demonstrate a residual tracking error of 490 nm rms in sample-motion direction, corresponding to a performance increase by factor 32, as compared to the state-of-the-art approach. The analysis of the performed measurements shows an uncertainty reduction by one order of magnitude to 610 nm rms, enabling 3D measurements on a moving sample with sub-micrometer precision.

**Index Terms**—Mechatronics, inline measurement systems, 3D imaging.

## I. INTRODUCTION

For today's high-tech manufacturing industry, flexibility is a key aspect to meet global trends, such as resource-efficient production, as well as to rapidly respond to fluctuating market demands [1], [2]. This is accompanied by a steady increase in product quality, while further raising the production efficiency [3]. In this relation, robotic inline measurement systems are considered as key enablers to keep up with these global trends [4]. As a consequence of the increased demand for automation in the quality assessment steps during manufacturing [5], the integration of industrial robots (IRs) for inspection tasks has grown significantly in recent decades [6], [7].

Compared to conventional high-precision measurement tools, such as coordinate measuring machines, which may require multiple un-/loading steps for a single workpiece and are typically operating off-line, robotic measurement systems offer higher versatility due to their kinematic structure and the flexible integration into a production line, increasing the overall production efficiency [8], [9]. To not impair the throughput,

Manuscript received Month xx, 2xxx; revised Month xx, xxxx; accepted Month x, xxxx. The authors are with the Christian Doppler Laboratory for Precision Measurements in Motion, Automation and Control Institute (ACIN), Technische Universität Wien, 1040 Vienna. \*Matthias Laimer and Daniel Wertjanz contributed equally to this work. Corresponding author: laimer@acin.tuwien.ac.at

inspection processes have to be conducted within the existing production cycle time [10], [11]. Particularly in production systems such as the automotive sector, robotic measurement systems operating along assembly lines on moving objects are widely deployed [6], [10]. With repeatabilities down to tens of microns, IRs have successfully replaced single-purpose tools in many industries [7], [12].

However, the integration of robotic measurement systems into industrial applications with single or even sub-micrometer precision, such as required for the inspection of optics or stacked IC devices, is still an unsolved challenge [13], [14]. Part of this limitation is the finite stiffness of IRs, resulting from the serial link of multiple rigid bodies, making it hardly feasible to position or move the robot end effector with micrometer precision [7]. Similar to the limited positioning precision of IRs, environmental vibrations induced by industrial processes cause relative motion between the robotic end effector and the sample, which impairs the overall positioning performance [15].

To compensate for disturbing relative motion between an inline measurement system and a sample, an active sample-tracking approach can be employed [16]. Recently, a high-precision 3D measurement system has been proposed, which comprises a levitated measurement platform (MP) [17]. By means of feedback control, a contactless stiff link between sample and measurement tool is established, compensating relative motion in six degrees of freedom (DOFs). So far, the system uses a long-range coarse actuator to manually position the measurement tool relative to a static sample with arbitrary spatial orientation [17]. For the combined actuation of both positioning systems, dual stage actuation and control is a viable approach. Its applications range from precise machining [18], [19] to the positioning of high-precision wafer stages in the semiconductor industry [20]. To enable measurements on moving samples, it combines the long-range and flexible positioning capability of the coarse actuation system with the short-stroke positioning range of the high-precision actuator.

The contribution of this paper is the integrated design of a dual stage positioning system with six DOFs enabling the precise tracking of moving samples with sub-micrometer precision, such that high-resolution 3D measurements can be performed in motion. The concept and integrated design of the sample-tracking 3D measurement system is introduced in Section II, followed by a description of the experimental setup in Section III. Based on the identified IR dynamics, a tailored

IEEE TRANSACTIONS ON MECHATRONICS

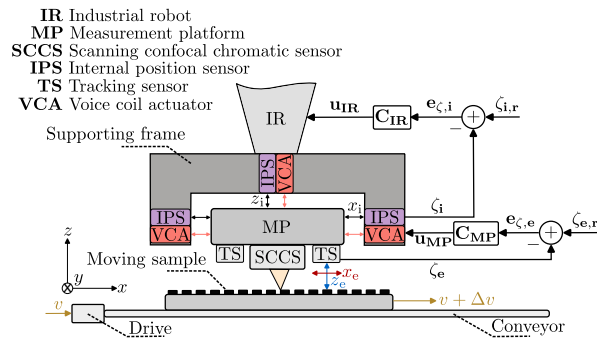


Fig. 1: Dual stage-controlled positioning system for precision measurements on moving samples. A constant relative position  $x_e$  and  $z_e$  between the MP and sample is maintained by the feedback controller  $C_{MP}$ . The feedback controller  $C_{IR}$  repositions the IR based on the internal MP positions  $x_i$  and  $z_i$ .

motion control scheme enabling the long-range tracking of moving samples is designed in Section IV. The tracking performance and the achieved 3D measurement precision in motion are evaluated in Section V. Finally, Section VI concludes this paper.

## II. INLINE 3D MEASUREMENTS ON MOVING OBJECTS

### A. System concept

The concept of the 3D measurement system for inline applications is shown in Fig. 1. With the sample being placed on a conveyor system, the total sample velocity  $v_S = v + \Delta v$  is a superposition of the process-induced conveyor velocity  $v$  and a disturbance-induced motion  $\Delta v$ . The sample-tracking 3D measurement module [21] is mounted as end effector to an IR. To compensate the disturbing relative motion between the scanning confocal chromatic sensor (SCCS) as 3D measurement tool (MT) and the moving sample, a dual stage concept is developed in a parent-child control architecture [22] in Section IV. The SCCS is embedded into an electromagnetically levitated MP, which is capable of tracking the sample with sub-micrometer precision [23]. In this relation, the MP is the precision and the IR the coarse positioning system. Tracking sensors (TSs) are integrated in the MP to measure the external position  $\zeta_e$  relative to the sample, i.e.  $x_e$  and  $z_e$  in Fig. 1. A constant relative position  $\zeta_{e,r}$  is maintained based on the measured deviation  $e_{\zeta,r}$  by means of feedback control ( $C_{MP}$ , with  $u_{MP}$  being the control output), establishing the desired stiff link between SCCS and sample.

Additional internal position sensors (IPSs) are integrated, which measure the MP's internal position  $\zeta_i$  relative to the IR. Based on the measured deviation  $e_{\zeta,i}$  from its center position  $\zeta_{i,r}$ , the IR is repositioned based on the control output  $u_{IR}$  of the feedback controller  $C_{IR}$ , such that the MP is kept within its limited actuation range. In this way, precise sample-tracking on the long-range is achieved, enabling the desired high-precision 3D measurements on moving objects.

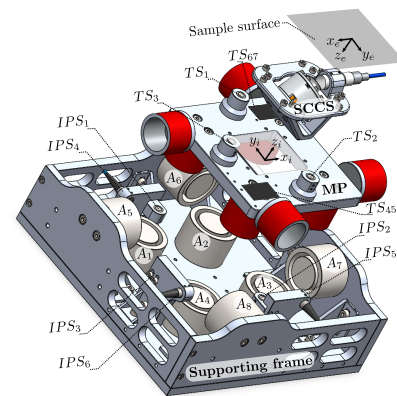


Fig. 2: Exploded view of the functional components of the 3D measurement module. A1 ... A8 are the VCAs to actuate the MP in all 6 DOFs. IPS1 ... IPS6 and TS1 ... TS6,7 are the internal position and tracking sensors, respectively. The SCCS is embedded into the MP as 3D MT

### B. Measurement module

Eight voice coil actuators (VCAR0087-0062-00 A, Supt-Motion, Suzhou, China), each capable of supplying 20 N continuous force as illustrated in Fig. 2, are integrated to enable quasi-zero stiffness actuation of the MP in six DOFs, which mechanically decouple it from disturbances induced by the limited positioning precision of the IR [17]. Voice coil actuators (VCAs) A1 - A4 are used to actuate the MP in its out-of-plane DOFs ( $z_i, \phi_{x_i}, \phi_{y_i}$ ), while the VCAs A5 - A8 enable the actuation in the in-plane DOFs ( $x_i, y_i, \phi_{z_i}$ ) [23]. With the MP being actuated within the air gaps (500  $\mu\text{m}$  between stator and mover) of the VCAs, an actuation range of about  $\pm 175 \mu\text{m}$  and  $\pm 3 \text{mrad}$  in the translational and rotational DOFs is achieved. Six capacitive IPSSm (IPS1 - IPS6, CSH05, Micro-Epsilon, Ortenburg, Germany), providing a measurement range of 500  $\mu\text{m}$  with 17 nm rms position noise at a measurement rate of 40 kHz, are used to measure the MP's position relative to the IR, which serves as feedback for the IR repositioning control ( $C_{IR}$  in Fig.1), being synthesized and discussed in detail in Section IV-B.

Three capacitive out-of-plane TS (TS1 - TS3, CSH05, Micro-Epsilon, Ortenburg, Germany) and two in-plane TSs based on photosensitive detectors (TS4,5 and TS6,7, S5991-01, Hamamatsu Photonics K.K., Hamamatsu, Japan) are integrated to measure the relative position between the MP and the sample in six DOFs [23]. To enable contactless high-precision 3D measurements, the embedded compact SCCS as described in [21] is used. It deploys a high precision 1D confocal chromatic sensor (IFS2404-2, Micro-Epsilon, Ortenburg, Germany) in combination with a 2D fast steering mirror (FSM) [24] to manipulate the optical path, enabling measurements in three dimensions. The spot diameter of the confocal chromatic sensor (CCS) is 10  $\mu\text{m}$ . The SCCS achieves a lateral and axial resolution down to 2.5  $\mu\text{m}$  and 77 nm within a measurement volume of 0.35 mm x 0.25 mm x 1.8 mm respectively, and frame rates of up to 1 fps. A more detailed

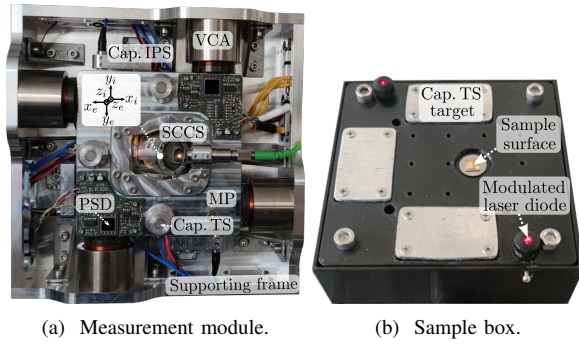


Fig. 3: Setup enabling high precision sample-tracking. (a) shows a detailed view of the sample-tracking measurement module with the SCCS as 3D measurement tool being embedded into the MP. (b) shows the sample box equipped with targets and markers for the out-of-plane and in-plane TSs [17].

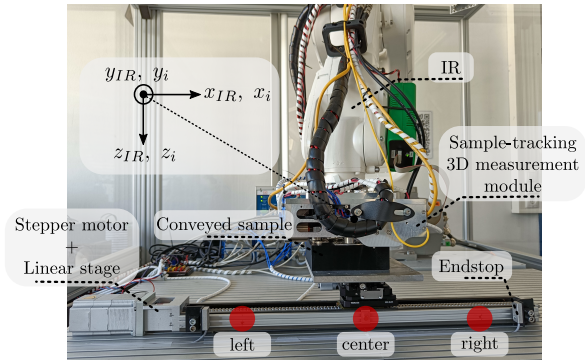


Fig. 4: Experimental setup of the dual stage positioning system for high-precision 3D measurements on moving samples. The long-range motion of the sample being conveyed by the linear stage is actively tracked using a dual stage control structure.

description can be found in [21].

The positioning uncertainty of the feedback-controlled MP is about 25 nm rms in the translational out-of-plane ( $z$ ) and about 200 nm rms in the translational in-plane DOFs ( $x$  and  $y$ ). With integrated aluminum targets for the capacitive sensors and modulated laser diodes (LDM650/1LJM, Roithner Lasertechnik GmbH, Vienna, Austria) as markers for the position sensitive detectors (PSDs), the sample box shown in Fig. 3b is used as the carrier of the sample surface to be inspected [23].

### III. EXPERIMENTAL SYSTEM SETUP

The sample-tracking 3D measurement module (see Fig. 3a) is mounted as end effector to the IR (KUKA KR 10 R900-2, KUKA AG, Augsburg Germany) with a working radius of 0.9 m. Figure 4 shows the experimental system setup. To emulate an industrial production line, a motorized 400 mm linear stage is used, with the two-phase stepper motor being actuated by a motor driver (TMC2209-V1.2, BIGTREETECH, Ltd., Shenzhen, China). By applying a frequency-modulated rectangular signal to the drive of the stepper motor, the conveyor velocity can be varied. The linear stage's velocity is mechanically limited to a maximum of  $15 \text{ mm s}^{-1}$ . As can be seen in Fig. 4, the IR's tool center point (TCP) and MP's internal coordinate system are selected to coincide in a common origin.

A rapid prototyping system (MicroLabBox, dSpace GmbH, Paderborn, Germany) is used for controlling the entire sample-tracking 3D measurement module. To enable the desired dual stage control of the robotic positioning system, a second, industrial DAQ system (components of Beckhoff Automation GmbH & Co. KG, Verl, Germany) is used, acquiring the internal MP position (see Fig. 1). The robot sensor interface (RSI, KUKA AG, Augsburg Germany) is used as real-time communication interface between the industrial DAQ system and the control unit of the IR, operating at a sampling frequency of 250 Hz (4 ms sampling time). It enables the repositioning of the IR's TCP based on external sensor signals and

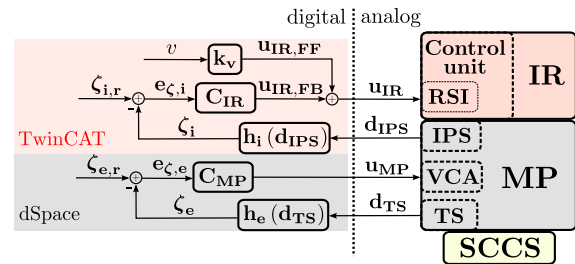


Fig. 5: Simplified block diagram of the dual stage-controlled robotic 3D measurement system. The SCCS is used as MT and integrated in the MP. The feedback controller  $C_{MP}$  is used to maintain a constant position between SCCS and the sample. Based on the measured internal MP position, the IR is repositioned by means of the feedback controller  $C_{IR}$  to maintain the MP within its limited actuation range.

allows the design and implementation of external control loops one level above the internal KUKA control. The IR reposition control is implemented on an engineering computer deploying TwinCAT 3 (Beckhoff Automation GmbH & Co. KG, Verl, Germany) and executed on an isolated physical processor core of the engineering PC with a sampling frequency of 12.5 kHz.

### IV. SYSTEM ANALYSIS AND CONTROL DESIGN

The measurement module in Fig. 3a comprises a 6-DOF SISO PID sample-control architecture, enabling the precise positioning of the MP relative to a sample [23]. A simplified block diagram of the dual stage positioning system is illustrated in Fig 5. Based on the measured tracking error  $e_{c,e}$ , the output  $u_{MP}$  of the sample-tracking controller  $C_{MP}$  is applied to the VCA-based actuation system. Embedded in the MP, the compact and lightweight SCCS is capable of performing high-precision 3D measurements [21].

To enable the tracking of moving samples on the long-range, the IR needs to be robustly and precisely repositioned in six

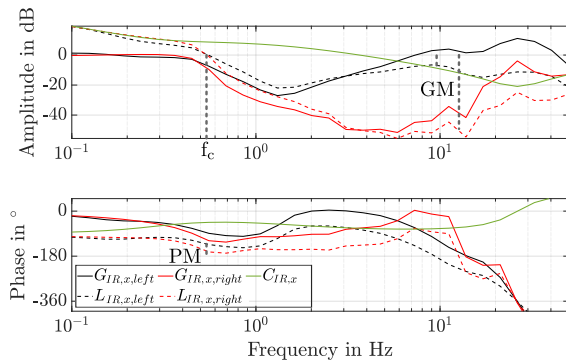


Fig. 6: Identification of the IR dynamics in motion direction (DOF  $x$ ) in the left and right IR position on the conveyor system ( $G_{IR,x,left}$  and  $G_{IR,x,right}$ ). A pair of anti-resonance and resonance is identified in a frequency range of 1 to 30 Hz. A single controller  $C_{IR,x}$  is designed for the entire conveyor travel range.

DOFs based on the internal position data, such that the MP is maintained within its limited actuation range. Therefore, the IR dynamics are identified and a tailored IR repositioning control  $C_{IR}$  (see Fig. 5) is designed in the following subsections.

#### A. Identification of IR dynamics

With the integrated sample-tracking controller  $C_{MP}$  [23], the IR dynamics along the conveyor travel range are identified in a first step. Considering the IR as a rigid-body system, its dynamics vary for different poses [25], which is why the dynamics are identified in three positions (left, center and right) indicated in red in Fig. 4. Therefore, a sinusoidal sweep  $A \sin(2\pi f k)$  is consecutively applied to the reference position  $\zeta_{i,r}$  in each DOF of the position-controlled IR in the range of 0.1 Hz to 50 Hz, with the amplitude  $A$  being set to 10  $\mu\text{m}$  and 0.1 mrad for the translational and rotational DOFs, respectively. Throughout the identification process in a certain pose, the MP's sample-tracking control is enabled, i.e. a stiff link to the conveyor system is established.

The dynamics for each DOF of the IR are obtained by

$$G_{IR,j} = \frac{\zeta_{i,j}}{\zeta_{i,j,r}}, \quad j \in \{x, y, z, \phi_x, \phi_y, \phi_z\}, \quad (1)$$

with  $\zeta_{i,j}$  being the MP's internal position in DOF  $j$  and  $\zeta_{i,j,r}$  the IR reference position. The identified IR dynamics are exemplarily shown for the motion direction  $x$  in Fig. 6 (solid black and red lines) at the left and right IR position on the conveyor system. As can be seen, a pair of anti-resonance and resonance is identified within the frequency range of 1 to 30 Hz in both poses, caused by the mechanical decoupling of the harmonic drive gears in the joints [26], [27]. The crosstalk between the individual DOFs of the IR for frequencies up to 0.5 Hz is 10 dB lower than the respective system dynamics (data not shown), which is why a single input single output (SISO) control architecture is pursued in the following controller synthesis.

#### B. Dual stage control design

Based on the identified IR dynamics, a SISO PI control architecture is designed one level above the internal KUKA control. The discretized PI control for the  $k^{\text{th}}$  time step in standard form [28]

$$u_{IR}(k) = k_p \left( e_{\zeta,i}(k) + \frac{T_s}{T_i} \sum_{l=0}^k e_{\zeta,i}(l) \right) \quad (2)$$

is synthesized for each DOF, with  $k_p$  being the proportional gain,  $T_i$  integrator time constant and  $T_s$  the corresponding sampling time. Since the Robot Sensor Interface (RSI) cycle time is 4 ms (cycle frequency is 250 Hz) but the internal MP's internal position signals are acquired with a sampling time of 80  $\mu\text{s}$ , the IR repositioning error  $e_{\zeta,i}$  is oversampled by a factor of 50, allowing moving averaging of  $e_{\zeta,i}$  to smooth higher frequency components.

As can exemplarily be seen in the identified dynamics  $G_{x,left}$  and  $G_{x,right}$  in Fig. 6, similar magnitudes and phases below the anti-resonance for the left and right IR position on the conveyor system are obtained, enabling the use of the same PI parameters for the IR repositioning along the entire conveyor range. The six individual controllers are synthesized in a loop-shaping approach based on the measured dynamics in the IR's center position (see Fig. 4). To suppress the excitation of the identified resonances without significantly impairing the phase margin, notch filters

$$H_{N,j}(s) = \frac{s^2 + 2\delta\pi\nu + 4\pi^2\nu^2}{s^2 + 2\delta\rho\pi\nu + 4\pi^2\nu^2}, \quad j \in \{x, y, z, \phi_x, \phi_y, \phi_z\}, \quad (3)$$

with  $\delta$  defining the width and  $\rho$  the depth at a certain frequency  $\nu$ , are designed for each DOF  $j$ . The resulting IR repositioning controller yields

$$C_{IR,j} = C_{PI,j} H_{N,j}, \quad j \in \{x, y, z, \phi_x, \phi_y, \phi_z\}, \quad (4)$$

with  $C_{PI,j}$  being the transfer function of the designed controller in Eq. 2 for a respective DoF  $j$ . Considering the conveyed sample motion direction (see Fig. 4), the highest IR control effort is required in DOF  $x$ . Therefore, a controller design trade-off is made, maximizing the cross-over frequency under the aspect of still providing a robust IR controller over the entire conveyor travel range. A cross-over frequency  $f_c$  of 550 mHz yields a robust gain and phase margin of 14 dB and 45°, respectively, for the IR being in the center position. As shown in Fig. 6, the phase margin (PM) decreases to 20°, while traveling towards the right position on the conveyor system. In the left position, the phase margin increases up to 50°.

For the remaining DOFs, lower IR repositioning control effort is expected. To keep the crosstalk between the axes at a minimum, sufficient PM and gain margin (GM) of at least 50° and 10 dB for the translational DOFs and 100° and 10 dB for the rotational DOFs are targeted in the controller synthesis.

The measured loop gain of the IR repositioning  $L_{IR,j}$  and the sample-tracking controller  $L_{MP,j}$ ,  $j \in \{x, y, z, \phi_x, \phi_y, \phi_z\}$  in the translational and rotational DOFs are presented in Fig. 7. As can be seen, each loop gain of the 6-DOF sample-tracking control is designed with a cross-over

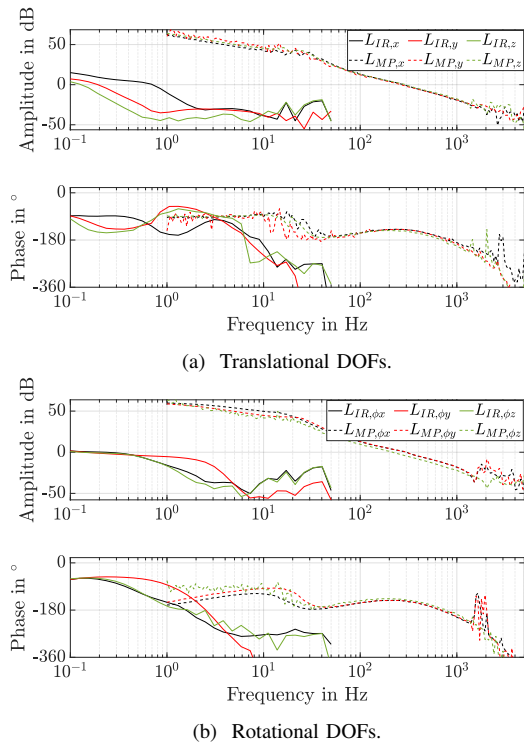


Fig. 7: Measured loop gain of the designed 6-DOF dual stage control. a) shows the loop gain of the translational and b) the rotational DOFs. The cross-over frequencies of the IR repositioning and the sample-tracking controllers are spectrally separated by about three decades.

frequency of about 300 Hz. The measured crossover frequencies as well as the PMs and GMs are summarized in Table I. A  $-3$  dB IR repositioning and sample-tracking bandwidth (BW) of about 1 Hz and 450 Hz is achieved, respectively.

To further increase the performance of the IR repositioning control, the *a priori* knowledge of the conveyor velocity is considered by an additional feedforward controller (see Fig. 5). The constant  $k_v$  converts the conveyor reference velocity  $v$  into an IR position signal for each cycle. The resulting control output  $\mathbf{u}_{IR}$  is a superposition of the feedback  $\mathbf{u}_{FB}(\mathbf{k})$  and the feedforward controller output  $\mathbf{u}_{FF}(\mathbf{k})$ .

## V. EXPERIMENTAL PERFORMANCE EVALUATION

For the performance evaluation of the dual stage-controlled system, the measurement module is aligned to the sample box (see Fig. 4), i.e. all TSs are in range. To enable a performance comparison with state-of-the-art robotic measurement systems, a benchmark scenario is defined. In a state-of-the-art robotic measurement system without MP, the MT is directly mounted to an IR. This is equivalent to mechanically fixing the MP with the robot arm and disabling the sample-tracking control. The integrated TS can then be used as a measure for the relative motion. Due to the measurement range of the out-of-plane sensors of  $500 \mu\text{m}$ , operation with entirely disabled

TABLE I: Measured cross-over frequencies, gain and phase margins. a) for the translational and b) for the rotational DOFs of the IR repositioning (center position) and the sample-tracking controller.

(a) Translational DOFs.

DOF	IR repositioning			Sample-tracking		
	$f_c$	GM	PM	$f_c$	GM	PM
x	0.55 Hz	14 dB	45°	289 Hz	16 dB	41°
y	0.18 Hz	11 dB	60°	284 Hz	15 dB	40°
z	0.11 Hz	12 dB	55°	301 Hz	12 dB	35°

(b) Rotational DOFs.

DOF	IR repositioning			Sample-tracking		
	$f_c$	GM	PM	$f_c$	GM	PM
$\phi_x$	0.34 Hz	23 dB	113°	302 Hz	12 dB	36°
$\phi_y$	0.14 Hz	12 dB	124°	303 Hz	12 dB	33°
$\phi_z$	0.14 Hz	23 dB	128°	225 Hz	18 dB	43°

tracking control is, however, not possible. For this reason, a relaxed benchmark scenario is used. The sample-tracking control bandwidth is reduced to 1 Hz, which keeps the sensors in range but essentially disables the disturbance rejection. The lateral sample motion tracking is disabled but robot-related oscillations are still suppressed due to the quasi-zero stiffness actuated MP. The relaxed benchmark scenario with 1 Hz tracking bandwidth thus already represents an improvement as compared to the actual state-of-the-art case.

## A. Dual stage-controlled tracking of a moving target

With consideration of the linear stage's maximum velocity of  $15 \text{ mm s}^{-1}$  (see Section III) and adding a sufficient safety margin, samples are conveyed with velocities of up to  $10 \text{ mm s}^{-1}$  to be robustly tracked. The 3<sup>rd</sup> order velocity trajectory shown in Fig. 8 is applied to the conveyor system, ensuring a smooth acceleration and deceleration phase. Within the time intervals  $[t_0, t_1]$  and  $[t_2, t_3]$ , the sample is accelerated from standstill up to  $v = 10 \text{ mm s}^{-1}$  and decelerated back to zero, respectively. In the interval  $[t_1, t_2]$ , the velocity  $v$  is kept constant for 10 s, serving as time slot for 3D measurements with the SCCS (see Section V-B). Since the MP actively tracks the sample motion, the RMS value of the internal MP position error can be used to quantify the performance of the dual stage-controlled robotic system. A value close to zero indicates that the MP is kept close to its center position, leaving a larger extent of the actuation range for tracking higher frequency disturbance-induced target motions. The IR repositioning and tracking performance of the dual stage-controlled robotic system is evaluated within the time interval  $T_{meas.} = [t_1, t_2] = 10 \text{ s}$ , i.e.  $v = \text{const}$ .

In Fig. 9, the IR's TCP motion as well as the MP's internal position and tracking error in six DOFs are shown for the applied velocity trajectory (see Fig. 8). As can be seen in Fig. 9a and 9b, an IR motion in all six DOFs is required to maintain the MP within its actuation range.

In sample motion direction (DOF  $x$ ), the IR is repositioned along a travelling range of more than 100 mm, indicated in black in Fig. 9a. Considering the MP's actuation range (see Section II-B), the system's tracking range is increased by

about three orders of magnitude. In the translational DOFs, the internal MP position error is kept below  $20\ \mu\text{m rms}$  (see Fig. 9c), leaving the MP almost 90% of the actuation range to track higher frequency sample motion. For a constant velocity  $v = 10\ \text{mm s}^{-1}$ , residual sample-tracking errors below  $500\ \text{nm rms}$  and  $200\ \text{nm rms}$  are achieved in the translational in- and out-of-plane DOFs (see Fig. 9e). The deviation in the tracking performance can be explained by the different sensing principles and the related noise floors of the in- and out-of-plane TSs (see Section II-B) [29]. Similar behavior can be recognized in the tracking error of the rotational DOFs (see Fig. 9f).

### B. High-precision 3D measurements in motion

To prove the feasibility of precision measurements on moving objects, the 3D measurement performance is evaluated, for (i) the defined benchmark scenario in Section V and (ii) the proposed dual-stage controlled positioning system. A silicon grating structure (Nanuler Calibration Standard, Applied NanoStructures Inc., Mountain view, CA, USA) with a pitch of  $20\ \mu\text{m}$  is used and placed on the sample box (see Fig. 3b). A microscope image of the sample under test is shown in Fig. 10a, with several surface defects located within the 3D measurement range. The measurement under static lab conditions is presented in Fig. 10b, with the grating pitch as well as the surface defects clearly visible. To achieve such conditions, the MP actively tracks the sample surface to compensate for disturbing relative motion between SCCS and the sample caused by environmental vibrations, while the IR is at standstill and mechanically braked. The SCCS conducts the 3D measurement point-by-point by scanning the sample surface with a Lissajous trajectory, achieving a framerate of  $0.1\ \text{fps}$ . The parallelogram-shaped measurement range is caused due to the alignment of the CCS [21]. As can be seen in Fig. 10b the sample height cannot be correctly reconstructed, as the spot diameter of the CCS matches the gap width of the calibration grating. As an indicator for the axial 3D measurement performance, the height variation along the cross-section at  $y = 205\ \mu\text{m}$  is used.

The motion trajectory from Fig. 8 is applied to the conveyed sample. Within the interval  $T_{meas.} = [t_1, t_2]$ , the RMS

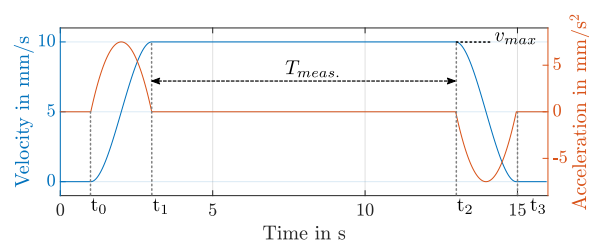


Fig. 8: Sample motion trajectory. Within the time interval  $[t_0, t_1]$ , the sample is accelerated from zero to a targeted velocity  $v_{max}$ . The sample velocity is kept constant for  $10\ \text{s}$  during the interval  $T_{meas.} = [t_1, t_2]$  before it gets decelerated back to zero during the interval  $[t_2, t_3]$ .

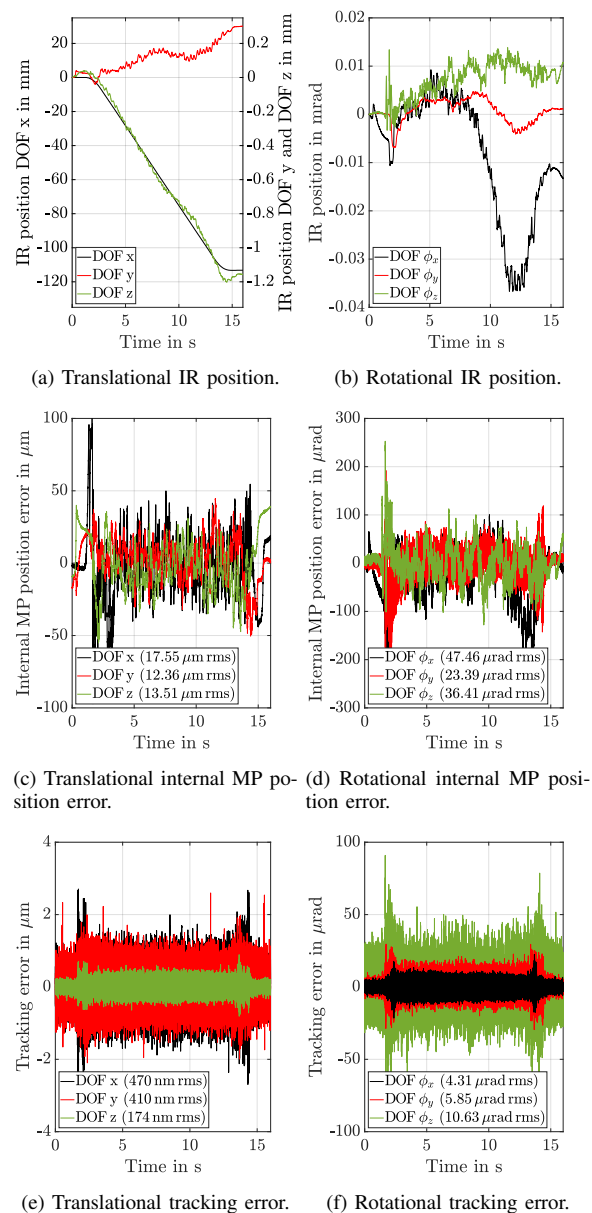
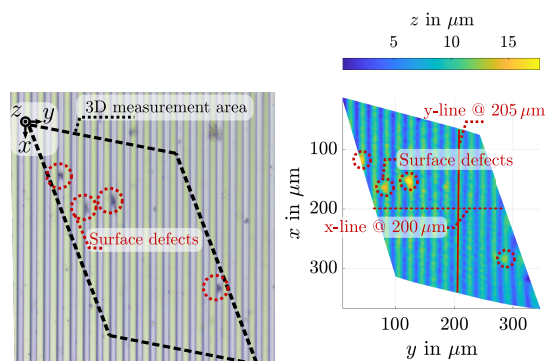


Fig. 9: Evaluated sample-tracking performance in 6-DOFs for the performed target motion trajectory of Fig. 8. (a, b) show the measured IR motion. (c, d) demonstrate the internal MP position error and (e, f) indicate the sample-tracking error in six DOFs.

tracking errors in motion direction (DOF  $x$ ) and out-of-plane (DOF  $z$ ) are evaluated for the maximum sample velocity  $v = 10\ \text{mm s}^{-1}$ . To demonstrate the effectiveness of the proposed dual stage-controlled sample-tracking system, a 3D measurement is acquired within this time interval.

Figure 11 shows the results of the 3D measurements in



(a) Microscope image.

(b) Lab measurement.

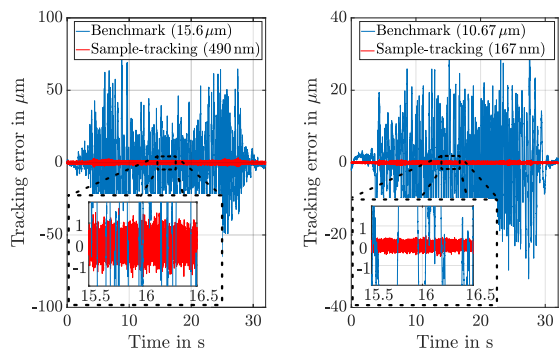
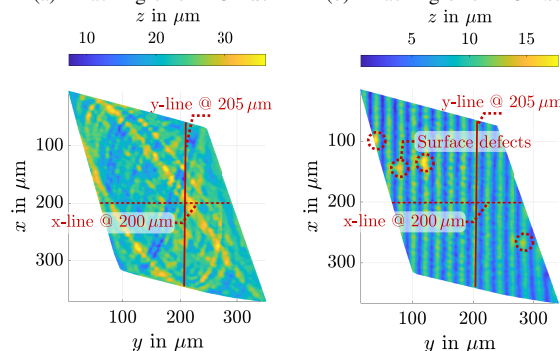
Fig. 10: Reference measurement of a test surface under laboratory conditions. a) shows a microscope image of the grating structure with a pitch of  $20\ \mu\text{m}$ . b) presents the 3D measurement under static, lab conditions (no disturbances and motion).

motion, with the tracking error exemplarily shown for the sample motion direction  $x$  (Fig. 11a) and the out-of-plane DOF  $z$  (Fig. 11b). In the benchmark scenario, as described at the beginning of Section V, tracking errors with RMS values of  $15.6\ \mu\text{m}$  in DOF  $x$  and of  $10.67\ \mu\text{m}$  in DOF  $z$  are obtained. The relative motion between the SCCS and the sample distorts the 3D measurement considerably (Fig. 11c).

To enable high-precision 3D measurements in motion, active sample-tracking is activated. The tracking error in Fig. 11a and 11b (red) is reduced to  $490\ \text{nm}$  rms in DOF  $x$  and of  $167\ \text{nm}$  rms in DOF  $z$ . This accords to a relative motion reduction by factors of 32 (motion direction  $x$ ) and 64 (DOF  $z$ ). The significantly reduced relative motion between SCCS and sample enables the precise 3D surface measurement on the moving sample (Fig. 11d).

By analyzing the axial measurement uncertainty (RMS value) along the top of the grating structure at  $y = 205\ \mu\text{m}$ , the 3D measurement performance is determined in Fig. 12. As can be seen, the high measurement uncertainty of  $10\ \mu\text{m}$  in the benchmark scenario (red) is in the same order of magnitude as the according tracking error in Fig. 11b. Compared to the benchmark scenario, the active sample-tracking reduces the 3D measurement uncertainty in motion (black) by one order of magnitude to  $610\ \text{nm}$  rms and, thus, close to the uncertainty of the static, lab conditions (dashed green). To evaluate the mean pitch, the grating structure is analyzed along  $x = 200\ \mu\text{m}$  for all three scenarios, as exemplarily shown in Fig. 10b. The mean pitch under static lab-like conditions is  $19.97\ \mu\text{m}$ , matching the pitch specified by the manufacturer. When performing 3D measurements on a moving sample with active sample-tracking, a mean pitch of  $19.46\ \mu\text{m}$  is obtained, showing a mean pitch measurement error of only  $500\ \text{nm}$ . As the grating structure cannot be reasonably reconstructed in the benchmark scenario for disabled sample-tracking, the pitch evaluation cannot be performed.

In summary, the dual stage-controlled positioning system re-

(a) Tracking error DOF  $x$ .(b) Tracking error DOF  $z$ .

(c) Benchmark.

(d) Tracking ON.

Fig. 11: Sample-tracking and 3D measurement performance for the sample conveyed at  $10\ \text{mm s}^{-1}$ . (a, b) show the sample-tracking performance in DOFs  $x$  and  $z$  with and without active sample-tracking control. Relative motion in the benchmark scenario corrupts the 3D measurement in c). For active sample-tracking in d), the grating structure and surface defects (see Fig. 10a) are visible.

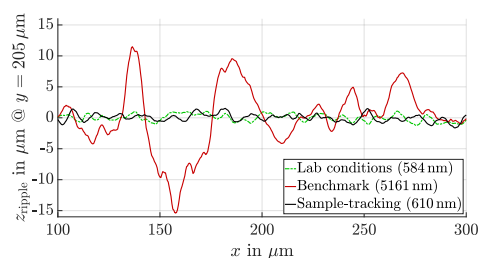


Fig. 12: Cross-sectional analysis of the 3D measurements in Fig. 10b (lab conditions), 11c (benchmark) and 11d (active sample-tracking). The active sample-tracking control reduces the 3D measurement uncertainty in motion (black) close to the uncertainty obtained in static, lab conditions (dashed green).

duces the long-range sample-tracking error by factor 32 down to  $490\ \text{nm}$  rms for velocities of up to  $10\ \text{mm s}^{-1}$ , enabling 3D measurements on moving objects with sub-micrometer precision.

## VI. CONCLUSION

This paper presents a dual stage-controlled 6-DOF positioning system to perform high-precision 3D measurements on samples in motion. The system comprises a sample-tracking measurement module mounted as end effector to a robotic coarse actuator. With a sample-tracking control BW of 450 Hz, the measurement module is capable of significantly reducing relative motion between the SCCS and the sample to perform 3D images with sub-micrometer precision. To maintain the MP within its actuation range while tracking a moving target in six DOFs, a dual stage control architecture is designed to reposition the robotic coarse actuator. The dynamics of the position-controlled robotic actuator are identified in different positions along the conveyor travel range. A 6-DOF robotic repositioning control with a BW of about 1 Hz is designed to enable the long-range tracking of moving samples. Experimental results at a sample velocity of  $10 \text{ mm s}^{-1}$  show, that compared to the benchmark scenario, the proposed sample-tracking approach reduces the tracking error in motion direction from  $15.6 \mu\text{m rms}$  to  $490 \text{ nm rms}$ . The analysis of the acquired 3D measurement data reveals a measurement uncertainty reduction by one order of magnitude to  $610 \text{ nm rms}$ , demonstrating the system's capability to perform 3D measurements with sub-micrometer precision on samples in motion. Compared to state-of-the-art robotic inline measurement systems, which typically achieve measurement accuracies in the range of tens of micrometers due to the finite positioning precision of IRs [11], [30], the proposed dual stage-controlled 6-DOF system effectively demonstrates the capability to perform inline measurements on moving objects. As a result, the achievable measurement precision is decoupled from the positioning accuracy of IRs. Future work will include extending the system's capability to perform 3D measurements on moving free-form surfaces, as it is often required in various industries, such as the automotive sector.

## VII. ACKNOWLEDGMENT

This project is partially funded by the Hochschuljubilaumsfonds of the city of Vienna, Austria under the project number H-260744/2020. The financial support by the Austrian Federal Ministry of Labour and Economy, the National Foundation for Research, Technology and Development and the Christian Doppler Research Association, and Micro-Epsilon Atensor GmbH and MICRO-EPSILON-MESSTECHNIK GmbH & Co.K.G. is gratefully acknowledged.

## REFERENCES

- [1] D. Imkamp, J. Berthold, M. Heizmann, K. Kniel, M. Peterek, R. Schmitt, J. Seidler, and K.-D. Sommer, "Herausforderungen und Trends in der Fertigungsmesstechnik – Industrie 4.0," *tm - Technisches Messen*, vol. 83, no. 7-8, pp. 417–429, 2016.
- [2] H. Lasi, P. Fettke, H.-G. Kemper, T. Feld, and M. Hoffmann, "Industry 4.0," *Business & information systems engineering*, vol. 6, no. 4, pp. 239–242, 2014.
- [3] D. Imkamp, R. Schmitt, and J. Berthold, "Blick in die Zukunft der Fertigungsmesstechnik," vol. 79, no. 10, pp. 433–439, 2012.
- [4] R. Schmitt and F. Moening, "Ensure success with inline-metrology," in *XVIII IMEKO World Congress - Metrology for a Sustainable Development*, 2006.
- [5] I. Iglesias, M. Sebastián, and J. Ares, "Overview of the state of robotic machining: Current situation and future potential," *Procedia Engineering*, vol. 132, pp. 911–917, 2015, mESIC Manufacturing Engineering Society International Conference 2015.
- [6] M. Bartoš, V. Bulej, M. Bohušik, J. Stanček, V. Ivanov, and P. Macek, "An overview of robot applications in automotive industry," *Transportation Research Procedia*, vol. 55, pp. 837–844, 2021, 14th International scientific conference on sustainable, modern and safe transport.
- [7] W. Ji and L. Wang, "Industrial robotic machining: A review," *International Journal of Advanced Manufacturing Technology*, vol. 103, pp. 1239–1255, 07 2019.
- [8] Y. Li and P. Gu, "Free-form surface inspection techniques state of the art review," *Computer-Aided Design*, vol. 36, no. 13, pp. 1395–1417, 2004.
- [9] S. Lemes, D. Strbac, and M. Cabaravdic, "Using industrial robots to manipulate the measured object in CMM," *International Journal of Advanced Robotic Systems*, vol. 10, no. 7, p. 281, 2013.
- [10] A. Tandiyi, S. Akthar, M. Moussa, and C. Tarray, "Automotive semi-specular surface defect detection system," in *2018 15th Conference on Computer and Robot Vision (CRV)*, pp. 285–291, 2018.
- [11] E. Kiraci, P. Franciosa, G. A. Turley, A. Olifent, A. Attridge, and M. A. Williams, "Moving towards in-line metrology: evaluation of a Laser Radar system for in-line dimensional inspection for automotive assembly systems," *The International Journal of Advanced Manufacturing Technology*, vol. 91, no. 1-4, pp. 69–78, 2016.
- [12] P. Shiakolas, K. Conrad, and T. Yih, "On the accuracy, repeatability, and degree of influence of kinematics parameters for industrial robots," *International journal of modelling and simulation*, vol. 22, no. 4, pp. 245–254, 2002.
- [13] F. Berry, R. Mermet-Lyauoz, J. M. Cuevas Davila, D. A. Djemmah, H. S. Nguyen, C. Seassal, E. Fourmond, C. Chevalier, M. Amara, and E. Drouard, "Light management in perovskite photovoltaic solar cells: A perspective," *Advanced Energy Materials*, vol. 12, no. 20, p. 2200505, 2022.
- [14] M. Liebens, A. Jourdain, J. De Vos, T. Vandeweyer, A. Miller, E. Beyne, S. Li, G. Bast, M. Stoerring, S. Hiebert, and A. Cross, "In-line metrology for characterization and control of extreme wafer thinning of bonded wafers," *IEEE Transactions on Semiconductor Manufacturing*, vol. 32, no. 1, pp. 54–61, 2019.
- [15] E. Csencsics, M. Thier, S. Ito, and G. Schitter, "Supplemental peak filters for advanced disturbance rejection on a high precision endeffector for robot-based inline metrology," *IEEE/ASME Transactions on Mechatronics*, p. 1, 2021.
- [16] Markus Thier, Rudolf Saathof, Andreas Sinn, Reinhard Hainisch, and Georg Schitter, "Six degree of freedom vibration isolation platform for in-line nano-metrology," *IFAC-PapersOnLine*, vol. 49, no. 21, pp. 149–156, 2016.
- [17] D. Wertjanz, E. Csencsics, T. Kern, and G. Schitter, "Bringing the lab to the fab: Robot-based inline measurement system for precise 3-D surface inspection in vibrational environments," *IEEE Transactions on Industrial Electronics*, vol. 69, no. 10, pp. 10666–10673, 2022.
- [18] B.-S. Kim, J. Li, and T.-C. Tsao, "Two-parameter robust repetitive control with application to a novel dual-stage actuator for noncircular machining," *IEEE/ASME Transactions on Mechatronics*, vol. 9, no. 4, pp. 644–652, 2004.
- [19] W. Dong, J. Tang, and Y. ElDeeb, "Design of a linear-motion dual-stage actuation system for precision control," *Smart Materials and Structures*, vol. 18, no. 9, p. 095035, Aug. 2009.
- [20] H. Lan, Y. Ding, H. Liu, and B. Lu, "Review of the wafer stage for nanoimprint lithography," *Microelectronic Engineering*, vol. 84, no. 4, pp. 684–688, 2007.
- [21] D. Wertjanz, T. Kern, E. Csencsics, G. Stadler, and G. Schitter, "Compact scanning confocal chromatic sensor enabling precision 3-D measurements," *Applied Optics*, vol. 60, no. 25, pp. 7511–7517, Sep. 2021.
- [22] L. Guo, D. Martin, and D. Brunnett, "Dual-stage actuator servo control for high density disk drives," in *1999 IEEE/ASME International Conference on Advanced Intelligent Mechatronics (Cat. No.99TH8399)*, pp. 132–137, 1999.
- [23] D. Wertjanz, T. Kern, A. Pechhacker, E. Csencsics, and G. Schitter, "Robotic precision 3D measurements in vibration-prone environments enabled by active six dof sample-tracking," in *2022 IEEE/ASME International Conference on Advanced Intelligent Mechatronics (AIM)*, pp. 1441–1446, 07 2022.
- [24] E. Csencsics, J. Schlarp, T. Schopf, and G. Schitter, "Compact high performance hybrid reluctance actuated fast steering mirror system," *Mechatronics*, vol. 62, p. 102251, 2019.

- [25] A. Karim, J. Hitzer, A. Lechler, and A. Verl, "Analysis of the dynamic behavior of a six-axis industrial robot within the entire workspace in respect of machining tasks," in *2017 IEEE International Conference on Advanced Intelligent Mechatronics (AIM)*, pp. 670–675, 2017.
- [26] J. Oaki, "Rigid-joint-model feedforward with elastic-joint-model feedback for motion control of a 6-dof industrial robot," *IFAC-PapersOnLine*, vol. 53, no. 2, pp. 8462–8469, 2020, 21st IFAC World Congress.
- [27] M. Chan, "Controller Synthesis and Vibration Suppression Techniques for Industrial Robotic Manipulators with Joint Flexibilities," Ph.D. dissertation, 2013.
- [28] S. Chander, P. Agarwal, and I. Gupta, "Auto-tuned, discrete PID controller for DC-DC converter for fast transient response," in *India International Conference on Power Electronics 2010 (IICPE2010)*, pp. 1–7, 2011.
- [29] D. Wertjanž, E. Csencsics, and G. Schitter, "An efficient control transition scheme between stabilization and tracking task of a MAGLEV platform enabling active vibration compensation," in *2020 IEEE/ASME International Conference on Advanced Intelligent Mechatronics (AIM)*, pp. 1943–1948, 2020.
- [30] H. Kihlman, R. Loser, A. Cooke, A. Sunnanbo, and K. Von Arb, "Metrology-integrated industrial robots: calibration, implementation and testing," in *35th ISR International Symposium on Robotics, 23-26 March, Paris, France*, pp. 1–6, 2004.



**Matthias Laimer** is doctoral researcher at the Automation and Control Institute (ACIN) at TU Wien, Vienna, Austria. He received an MSc. degree in Electrical Engineering from TU Wien in 2022. His primary research interests are on industrial automation, and robot-based inline measurement systems.



**Daniel Wertjanž** is doctoral researcher at the Automation and Control Institute (ACIN) at TU Wien, Vienna, Austria. He received an MSc. degree in Electrical Engineering from TU Wien in 2019. His primary research interests are on high-performance mechatronic systems design, high-precision motion control, and robot-based inline measurement systems.



**Peter Gsellmann** is doctoral researcher at the Automation and Control Institute (ACIN) at TU Wien, Vienna, Austria. He received an MSc. degree in Electrical Engineering from TU Wien in 2018. His primary research interests are on industrial automation, and vision-based control of industrial robots.



**Georg Schitter** is Professor for Advanced Mechatronic Systems at the Automation and Control Institute (ACIN) of TU Wien. He received the MSc. degree in electrical engineering from TU Graz, Graz, Austria, in 2000 and the second MSc. degree in information technology and PhD. degree in technical sciences from ETH Zurich, Zurich, Switzerland, in 2004. His primary research interests are on high-performance mechatronic systems, particularly for applications in the high-tech industry, scientific instrumentation, and mechatronic imaging systems, such as AFM, scanning laser and LIDAR systems, telescope systems, adaptive optics, and lithography systems for semiconductor industry. He received the journal best paper award of IEEE/ASME Transactions on Mechatronics (2018), of the IFAC Mechatronics (2008-2010), of the Asian Journal of Control (2004-2005), and the 2013 IFAC Mechatronics Young Researcher Award. He served as an Associate Editor for IFAC Mechatronics, Control Engineering Practice, and for the IEEE Transactions on Mechatronics.



**Ernst Csencsics** is Associate Professor for Measurement Systems at the Automation and Control Institute (ACIN) of TU Wien. He received an MSc. and a PhD degree (sub auspiciis) in Electrical Engineering from TU Wien, Austria in 2014 and 2017, respectively. His primary research interests are on opto-mechatronic measurement and imaging systems, high performance mechatronics, scientific instrumentation, precision engineering, and advanced robotic inline measurement systems. He received the journal Best Paper Award of IEEE/ASME Transactions on Mechatronics (2018), the Best Paper Award at the IEEE International Instrumentation and Measurement Technology Conference (2022) and the Best Student Paper Award at the American Control Conference (2016).